Apparent directional spectral emissivity determination of semitransparent materials*

Chun-Yang Niu(牛春洋), Hong Qi(齐宏)†, Ya-Tao Ren(任亚涛), and Li-Ming Ruan(阮立明)

School of Energy Science and Engineering, Harbin Institute of Technology, Harbin 150001, *China*

(Received 13 November 2015; revised manuscript received 14 December 2015; published online 25 February 2016)

An inverse estimation method and corresponding measurement system are developed to measure the apparent spectral directional emissivities of semitransparent materials. The normal spectral emissivity and transmissivity serve as input for the inverse analysis. Consequently, the refractive index and absorption coefficient of the semitransparent material could be retrieved by using the pseudo source adding method as the forward method and the stochastic particle swarm optimization algorithm as the inverse method. Finally, the arbitrary apparent spectral directional emissivity of semitransparent material is estimated by using the pseudo source adding method given the retrieval refractive index and absorption coefficient. The present system has the advantage of a simple experimental structure, high accuracy, and excellent capability to measure the emissivity in an arbitrary direction. Furthermore, the apparent spectral directional emissivity of sapphire at 773 K is measured by using this system in a spectral range of 3 μm–12 μm and a viewing range of 0°–90°. The present method paves the way for a new directional spectral emissivity measurement strategy.

Keywords: semitransparent materials, inverse problem, directional emissivity

PACS: 78.20.Ci, 02.30.Zz, 44.40.+a, 45.10.Db **DOI:** 10.1088/1674-1056/25/4/047801

1. Introduction

The emissivity is defined as the ratio between the amount of radiation emitted by an object and that emitted by a perfect blackbody, at the same temperature and under the same geometrical and spectral conditions.[1] As a fundamental optical property, the emissivity of a material is usually strongly dependent on wavelength. As a relative physical parameter that defines the way an object emits thermal electromagnetic radiation,[2] the spectral emissivity plays an essential role in temperature measurements using radiation thermometers and in the analysis of the radiative heat transfer between objects.[3] Moreover, the spectral emissivity is highly influenced by the surface state, and depends on surface material geometry (i.e., curvature and roughness), material composition, oxidation, surface contamination, impurity, coating, thermal uniformity, etc. In other words, the spectral emissivity is a multivariate function of such factors. In particular, for a semitransparent material, due to the volumetric absorbing and scattering characteristics, the emissivity of semitransparent material is an apparent physical quantity, which strongly depends on the thickness of material and the above influence factors, and needs special consideration.

For emissivity as an important physical parameter that represents the radiative capability of materials, its accurate behavior in a wide range of wavelength and direction is of particular interest and indispensable to many applications such as remote sensing, solar energy utilization, and high-temperature measurements.[4–14] Taking non-contact high-temperature measurement (pyrometry) for example, accurate knowledge of the emissivity is required to evaluate the true temperature of a sample from the so-called radiance temperature. Uncertainty in the emissivity is the principal source of errors in determining the surface temperature from the infrared radiation measurements. Therefore, the first and most essential stage in solving the non-contact temperature measurement problems is to determine the spectral emissivity of the material accurately. In recent years, the semitransparent optical window materials, such as quartz, sapphire, zinc sulfide (ZnS), or silicon, ceramic, and inorganic composite materials, have attracted significant attention for their wide potential applications in solar heat receiver, spacecraft photoelectric detection, high-temperature measurement technology, and thermophotovoltaic applications.[5–8] The spectral emissivity values of these semitransparent materials are fundamental data of engineering design and the analyses of thermal processes and radiative transfers, which have important implications for the development of relevant engineering technology and scientific research.[9] Until now, accurate determination of the directional spectral emissivity of these semitransparent materials is still an open problem.

To accurately measure the spectral emissivity values of various materials, much effort has been made in the past several decades. Typically, the emissivity measurement approaches can be classified as two main types, namely the indi-

*Project supported by the National Natural Science Foundation of China (Grant Nos. 51476043 and 51576053) and the Foundation for Innovative Research Groups of the National Natural Science Foundation of China (Grant No. 51421063).

†Corresponding author. E-mail: qihong@hit.edu.cn

© 2016 Chinese Physical Society and IOP Publishing Ltd

rect or direct method.[15,16] The indirect measurement method is based on the measurements of other quantities related to emissivity, and these quantities can be calorimetric or radiometric. For instance, Worthing *et al.*[4] developed the simplest steady-state calorimetry (the filament heating method) for measuring the full wavelength hemispherical emissivity. This method however can only measure the full spectrum hemispherical emissivity.[4] Cezairliyan and Laylor[10] first established the pulse heating transient calorimetric device based on the integrating sphere reflectometry method for measuring eight thermal physical property parameters including the emissivity. Fu *et al.*[17] and Fu and Tan[18] developed two types of total hemispherical emissivity devices for conductive materials based on steady-state calorimetry and transient calorimetry, respectively. Consequently, the influences of surface condition, including surface roughness and oxidation state, on the total hemispherical emissivity were investigated by using improved steady-state calorimetry for iron-based alloy samples.[19] Moreover, they also developed a new method to simultaneously measure the total hemispherical emissivity and the thermal conductivity of a sample at high temperature by using steady-state calorimetry.[20] For direct measurement, emissivity is determined by comparing the emission from a sample with that from a blackbody at the same temperature and wavelength, both emissions are measured with the same detector over an identical or equivalent optical path. Since the 1990s, with the development and wide use of the Fourier transform infrared (FTIR) spectrometer, many researchers have used it to directly measure the emissivities. Lindermeir *et al.*[21] and Tank[22] employed the FTIR spectrometer in a direct measurement device which could measure the emissivities and temperatures of opaque materials simultaneously. The measured spectral range however is 1.3 μm–5.4 μm, the measured temperature is less than 500 K, and the maximum resolution of the spectrometer is 0.5 cm^{-1}. Obviously, these device ranges are quite limited. Subsequently, Dai *et al.*[23] developed a direct measurement system of spectral emissivity, which was incorporated into an FTIR spectrometer, and extended the measured spectral range and temperature range significantly. The measurement spectral range reaches 0.6 μm–25 μm, and the measured temperature range is 333 K–1773 K.

Most of the emissivity measurement technologies introduced above are limited to opaque materials because the radiation from opaque material is only surface radiation and easily measured accurately. More recently, with the development of optical measurement and materials science, the emissivity measurements of semitransparent materials have become more and more urgent. Rigorous analyses of their radiation behaviors are hampered due to the lack of accurate values of the directional spectral emissivity. For instance, Sova *et al.*[24] developed a vacuum emissivity measurement device for semitransparent materials. A carbon dioxide laser was used to heat samples and the FTIR spectrometer was applied to measure the spectral radiant energy. The two-color pyrometer was used to measure the temperature of the sample. The spectral normal emissivity values of sapphire, spinel, yttria, and fused silica over the range 600 K–2000 K were measured with this device in a wave number range of 500 cm^{-1}–5000 cm^{-1}. González–Fernández *et al.*[25] used a highly accurate homemade infrared radiometer to measure the spectral normal emissivity values of atmospheric plasma sprayed (PS) YSZ films layered on Inconel 718 substrates at 603 K–1003 K based on the direct method, and the spectral range is 2.5 μm–22 μm. Rozenbaum and Meneses[26] developed a spectral directional emissivity measurement device by using a carbon dioxide laser to heat semitransparent samples. The temperatures of the samples could reach 3000 K, and the wave number range is 10–12000 cm^{-1}. The viewing direction of the measured directional emissivity by this device was limited to a range from the normal to 60°. Lee *et al.*[27] developed a two-substrate method to measure the spectral directional emissivity values of semitransparent materials based on the FTIR spectrometer, and the spectral directional emissivity of alumina. However, the viewing direction was limited within a range from the normal to 50°.

In summary, most of the current emissivity measurement techniques focused on dealing with opaque materials, and most of the experimental devices could only measure the normal emissivity values. To the best of our knowledge, only a few experimental investigations have been reported on the spectral directional emissivity measurement technology for semitransparent materials. However, the existing spectral directional emissivity measurement technology for semitransparent materials is disadvantaged by limited measuring view scope and complex experimental assemblies. The directional spectral emissivities of semitransparent materials have not been thoroughly investigated and a systematic study of the directional spectral emissivity as a function of the temperature has not been found either. With this idea, the main purpose of the present work is to develop an accurate measurement technique to determine the apparent spectral directional emissivities of semitransparent materials by combining the normal spectral emissivity measurement technique for semitransparent materials with an inverse estimation method. This technique has the advantages of simple structure, high accuracy, and the excellent capability to measure the emissivity in an arbitrary direction, so that it can be widely used to measure the apparent spectral directional emissivities of various semitransparent materials. The remainder of the present study is organized as follows. The measurement principle and devices

are described in Section 2. The measurement system is verified in Section 3. The apparent spectral directional emissivity measurement results of sapphire are analyzed in Section 4. In Section 5, the main conclusions are given.

2. Measurement principle and experimental apparatus

To measure the arbitrary directional spectral emissivities of semitransparent materials accurately, an inverse estimation method and the corresponding measurement system are developed. The whole technical procedure can be summarized as follows. Initially, the apparent normal spectral emissivity $\varepsilon_{\perp}(\lambda,T)$ and transmissivity $\tau(\lambda,T)$ of the sample at the required temperature T are measured by the normal spectral emissivity measurement device. Then, with the measured emissivity and transmissivity data, the refractive index $n(\lambda,T)$ and absorption coefficient $\kappa(\lambda,T)$ of the sample are retrieved by using the pseudo source adding (PSAD) method as the direct method and the stochastic particle swarm optimization (SPSO) algorithm as the inverse method. Finally, the apparent spectral directional emissivity of the semitransparent material is predicted by the PSAD method with the input of the retrieval refractive index and absorption coefficient. In this measurement system, the measurement temperature is in a range of 300 K–1773 K, the spectral range is 2.5 μm–25 μm, and the viewing range is 0°–90°. The detailed procedures of the present technology are as shown below.

2.1. Apparent normal spectral emissivity measurement apparatus

The basic principle of emissivity measurement based on the direct method is to measure the radiation energy in the normal direction of the material itself and the radiation energy in the normal direction of a reference blackbody at the same temperature; the ratio between the two values is the apparent normal emissivity of material. However, the background radiation noise and the transmission of semitransparent material make it difficult to measure the radiation energy of material itself directly, which brings great difficulty in measuring the apparent emissivity of semitransparent material. So an apparent normal spectral emissivity measurement apparatus for semitransparent material and the corresponding correction method are developed to deduce the background radiation noise first, from which the apparent normal spectral emissivity and transmissivity can be simultaneously measured. Figure 1 shows a schematic of the measurement apparatus.

The emissivity measurement system is composed of an FTIR spectrometer, reference blackbody, heating furnace and its temperature control system, infrared light source, control and data processing system, and diaphragm. A standard blackbody is used for the radiometer calibration, and an FTIR spectrometer is used as a radiation detector. The furnace is heated using a silicon molybdenum heater which is controlled by a proportional-integral-derivative temperature control system. The spectrometer is fixed on an optical lift platform, which can be rotated freely from 0° to 360°. A diaphragm controls the amount of light, which is mainly used for adjusting the strength of the passing light. The high pressure mercury lamp or blackbody can be employed as an infrared source, and a high-temperature blackbody furnace is used as an infrared source in the present study. The distance between the infrared light source and the sample is $L_1 = 700$ mm, the distance between the FTIR and the sample is $L_2 = 300$ mm, the distance between the FTIR and the blackbody is $L_3 = 300$ mm, the size of the heating furnace is 200 mm×200 mm×200 mm, and the diameter of the sample is 30 mm. It is worth noting that the blackbody and the sample should be viewed by the same detector over an equivalent optical path. The detailed information about the main experimental devices is listed in Table 1.

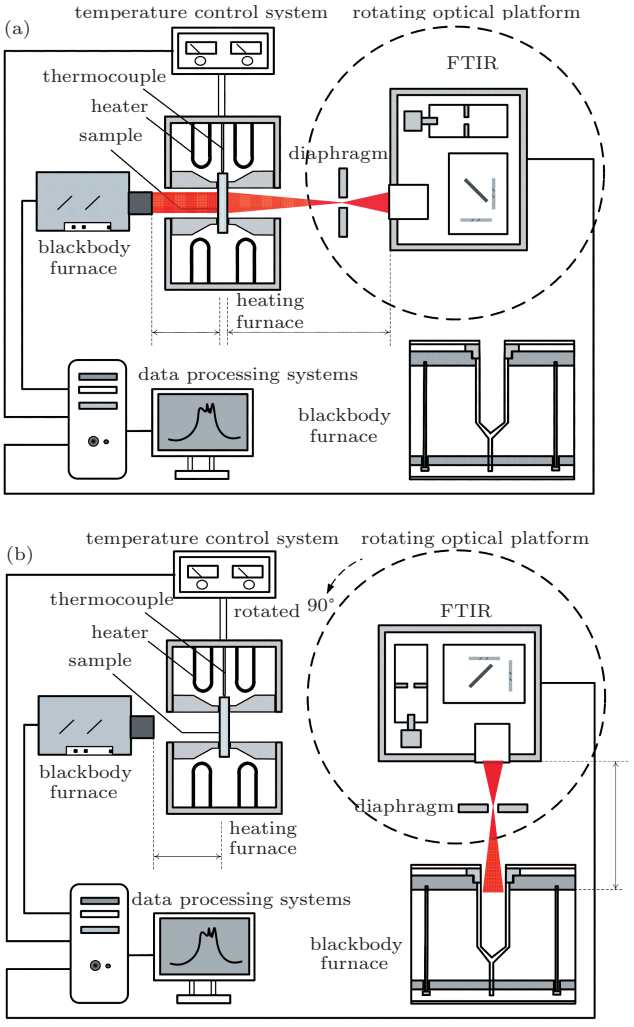


Fig. 1. (color online) Schematic diagrams of the apparent normal emissivity measurement apparatus. (a) Radiative signal collection of the sample and (b) radiative signal collection of the blackbody.

Table 1. Detailed information about the main experimental devices.

Device name	Model	Origin	Main parameter
FTIR spectrometer	FTIR-6100	Japan	The highest spectral resolution: 0.022 nm Spectral range: 1.25 μm–25 μm
Blackbody	RT1500	U. K.	T_{max}: 1450° The effective emissivity: 0.995
Furnace and temperature control system	SGM.M6/14AE	China	Heating power: 4 kW T_{max}: 1700 °C

2.2. Apparent normal spectral emissivity and transmissivity measurement principle

2.2.1. Calibration method of deducting background radiation noise

Assuming a linear response for the FTIR spectrometer to incident spectral radiance (indeed, its nonlinear response contributes to approximately 0.5% error[28] which can be approximated as a linear response), the measurement spectral radiation signal can be expressed as

$$S(\lambda) = S'(\lambda) + S_0(\lambda), \tag{1a}$$

$$S'(\lambda) = R(\lambda)G_1(\lambda)I(\lambda, T), \tag{1b}$$

$$S_0(\lambda) = R(\lambda)G_2(\lambda)I_0(\lambda, T_0), \tag{1c}$$

where $G_1(\lambda)$ and $G_2(\lambda)$ are the spectral geometric factors of the sample and background, respectively, which depend on the geometry of the light path system; $R(\lambda)$ is the spectral response characterized by the properties of the optical and electrical component; $I(\lambda,\ T)$ denotes the incident spectral radiance of the sample; and $I_0(\lambda,\ T_0)$ represents the background radiance emitted from the instrument.

The purpose of the calibration is to determine the instrument functions $G_1(\lambda)R(\lambda)$ and $G_2(\lambda)R(\lambda)\cdot I_0(\lambda,\ T_0)$. As $I(\lambda,\ T)$ is an essential quantity in the output signal of the FTIR spectrometer, the value of $G_1(\lambda)R(\lambda)$ is calculated from Eq. (1). From Ref. [3], the reference blackbody furnace is set to be two temperatures T_1 and T_2, and the output signals of the FTIR spectrometer $S_{b1}(\lambda)$ and $S_{b2}(\lambda)$ can be expressed as

$$\begin{aligned}\begin{bmatrix} S_{b1}(\lambda) \\ S_{b2}(\lambda) \end{bmatrix} &= R(\lambda) \begin{bmatrix} G_1(\lambda) \\ G_2(\lambda) \end{bmatrix}^{\mathrm{T}} \begin{bmatrix} I_b(\lambda,T_1) & I_b(\lambda,T_2) \\ I_0(\lambda,T_0) & I_0(\lambda,T_0) \end{bmatrix} \\ &= \begin{bmatrix} S'_{b1}(\lambda)+S_0(\lambda) \\ S'_{b2}(\lambda)+S_0(\lambda) \end{bmatrix}, \end{aligned} \tag{2}$$

where $S'_{b1}(\lambda)$ and $S'_{b2}(\lambda)$ are the actual radiances of the blackbody furnace for temperatures T_1 and T_2, respectively; $I_b(\lambda,\ T)$ is the spectral radiation of the blackbody furnace at temperature T, which can be calculated by Planck's law:

$$I_b(\lambda,\ T) = \frac{c_1\lambda^{-5}}{\exp[c_2/(\lambda \mathrm{T})]-1}, \tag{3}$$

with $c_1 = 3.7418\times10^8$ W $\cdot$ μm^4/m^2 and $c_2 = 1.4388\times10^4$ μm $\cdot$ K being respectively the first and second radiation constant of Planck's law; $S_0(\lambda)$ reflects the functional relationship between the input and output signal of the FTIR spectrometer, which can be determined by the responsivities of the optical system, electronic circuit, and detector. $G_1R(\lambda)$ and $S_0(\lambda)$ can be obtained from Eq. (2) as follows:

$$G_1(\lambda)R(\lambda) = \frac{S_{b2}(\lambda)-S_{b1}(\lambda)}{I_b(\lambda,T_2)-I_b(\lambda,T_1)}, \tag{4}$$

$$\begin{aligned} S_0(\lambda) &= G_2(\lambda)R(\lambda)I_0(\lambda,T_0) \\ &= S_{b1}(\lambda) - \frac{[S_{b2}(\lambda)-S_{b1}(\lambda)]\,I_b(\lambda,T_1)}{I_b(\lambda,T_2)-I_b(\lambda,T_1)}. \end{aligned} \tag{5}$$

2.2.2. Measurement procedure of the apparent normal spectral emissivity and transmissivity

The critical problem of the apparent normal spectral emissivity and transmissivity measurement is to measure the radiative energy of the material itself in the normal direction. Therefore, the following measurement procedure is developed.

Step 1 Turn on the blackbody furnace for 30 min and adjust the collimation of the optical path. Measure the spectral radiation of the blackbody furnace at two temperatures (see Fig. 1(b)). Calculate the spectral response function of the FTIR spectrometer according to the above correction method to deduce the background radiation noise.

Step 2 Turn on the incident light source and collect spectral radiation signal $S_1(\lambda)$ by using the FTIR spectrometer (see Fig. 1(a)) on the rotating platform, which includes the required radiation signal of incident light source $S'_1(\lambda)$ and the radiation signal of the background $S_0(\lambda)$.

Step 3 Turn off the incident light source. Heat the furnace without a sample to the test-required temperature and keep the temperature steady. Record spectral radiation signal $S_2(\lambda)$(see Fig. 1(a)), which includes the radiation signal of the furnace $S'_2(\lambda)$ at the test-required temperature and the radiation signal of the background $S_0(\lambda)$.

Step 4 Place the sample in the furnace. Heat the semitransparent sample to the scheduled test temperature and keep the temperature steady. Record spectral radiation signal $S_3(\lambda)$ by using the FTIR spectrometer (see Fig. 1(a)), which includes the rest of the furnace radiation signal through the semitransparent sample, the radiation signal of the semitransparent sample itself $S'_s(\lambda)$ and the radiation signal of the background $S_0(\lambda)$.

Step 5 Turn on the incident light source and keep the sample temperature steady. Record spectral radiation signal $S_4(\lambda)$ by using the FTIR spectrometer (see Fig. 1(a)), which includes the rest of the radiation signal $S_1'(\lambda)$ and $S_2'(\lambda)$ through the semitransparent sample, the radiative signal of the semitransparent sample itself $S_s'(\lambda)$, and the radiation signal of the background $S_0(\lambda)$.

Step 6 Heat the blackbody furnace to the test temperature and keep the temperature steady. Rotate the optical platform to face the blackbody furnace and record spectral radiation signal $S_b(\lambda)$ of the blackbody furnace at the test temperature by using the FTIR spectrometer (see Fig. 1(b)).

According to the above steps, the equations for the radiative signals are

$$S_1(\lambda) = S_1'(\lambda) + S_0(\lambda), \tag{6a}$$

$$S_2(\lambda) = S_2'(\lambda) + S_0(\lambda), \tag{6b}$$

$$S_3(\lambda) = S_2'(\lambda)\tau(\lambda,T) + S_s'(\lambda) + S_0(\lambda), \tag{6c}$$

$$S_4(\lambda) = \left[S_1'(\lambda) + S_2'(\lambda)\right]\tau(\lambda,T) + S_s'(\lambda) + S_0(\lambda), \tag{6d}$$

where $\tau(\lambda,T)$ is the spectral transmissivity of the semitransparent sample at the test temperature.

The spectral transmissivity and the real radiation signal of the semitransparent sample itself $S_s'(\lambda)$ at the test temperature can be obtained from Eq. (6) as follows:

$$\tau(\lambda,T) = \frac{S_4(\lambda) - S_3(\lambda)}{S_1(\lambda) - S_0(\lambda)}, \tag{7}$$

$$S_s'(\lambda) = S_3(\lambda) - S_0(\lambda) - \frac{[S_2(\lambda) - S_0(\lambda)]\,[S_4(\lambda) - S_3(\lambda)]}{[S_1(\lambda) - S_0(\lambda)]}. \tag{8}$$

Combining Eqs. (1), (4), and (5), the spectral radiative intensity of the semitransparent sample becomes

$$I_s(\lambda,T) = \frac{S_s'(\lambda)}{G_1(\lambda)R(\lambda)} = \frac{S_3(\lambda) - S_0(\lambda)}{G_1(\lambda)R(\lambda)} - \frac{[S_2(\lambda) - S_0(\lambda)]\,[S_4(\lambda) - S_3(\lambda)]}{G_1(\lambda)R(\lambda)\,[S_1(\lambda) - S_0(\lambda)]}. \tag{9}$$

In addition, the spectral radiative intensity of the blackbody furnace is expressed as

$$I_b(\lambda,T) = \frac{S_b(\lambda) - S_0(\lambda)}{G_1(\lambda)R(\lambda)} = \frac{S_b(\lambda)}{G_1(\lambda)R(\lambda)} - \frac{G_2(\lambda)}{G_1(\lambda)} I_0(\lambda,T_0). \tag{10}$$

The normal spectral emissivity of the semitransparent sample without background noise interference is obtained from Eqs. (9) and (10) as follows:

$$\varepsilon_\perp(\lambda,T) = \frac{I_s(\lambda,T)}{I_b(\lambda,T)} = \frac{S_3(\lambda) - S_0(\lambda)}{S_b(\lambda) - S_0(\lambda)} - \frac{[S_2(\lambda) - S_0(\lambda)]\,[S_4(\lambda) - S_3(\lambda)]}{[S_b(\lambda) - S_0(\lambda)]\,[S_1(\lambda) - S_0(\lambda)]}, \tag{11}$$

where $S_1(\lambda)$, $S_2(\lambda)$, $S_3(\lambda)$, $S_4(\lambda)$, and $S_b(\lambda)$ are the radiative signals detected by the FTIR spectrometer respectively. $S_0(\lambda)$ can be calculated from Eq. (5).

In summary, the transmissivity and apparent normal spectral emissivity of semitransparent material can be obtained according to Eqs. (7) and (11).

2.3. Apparent spectral directional emissivity measurement principle

To determine the apparent spectral directional emissivity of semitransparent material, the values of the refractive index n and absorption coefficient over a wide spectral range are required to be known. In the present study, the apparent normal spectral emissivity and transmissivity measured by the measurement system serve as input for the inverse analysis. The spectral refractive indices and the absorption coefficients of the semitransparent material at different temperatures can then be retrieved by using the PSAD method as the forward method and using the SPSO algorithm as the inverse one. The apparent spectral directional emissivity of semitransparent material is then estimated by using the PSAD method with the retrieval refractive index and absorption coefficient.

2.3.1. Forward method

The PSAD method, first developed by Huang *et al.*[29,30] in 1999, enables the efficient and accurate calculation of the apparent directional emissivity of semitransparent medium with known refractive index and absorption coefficient. In the present study, this method is used as the forward method to calculate the apparent spectral emissivity and transmissivity which serve as input for the inverse analysis.

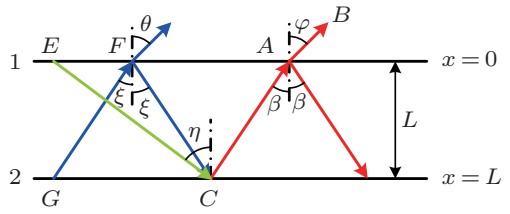


Fig. 2. Physical model of the PSAD.

A one-dimensional non-gray semitransparent medium slab (Fig. 2) is considered. The temperature is denoted by T, the thickness by L, the spectral refractive index by n_λ, and the spectral absorption coefficient by κ_λ. Assuming that interface 1 is the semitransparent and specular-emerging surface, the radiative transfer equation (RTE) for this medium can be expressed as

$$\frac{\mathrm{d}I_\lambda(\tau,s)}{\mathrm{d}\tau} + I_\lambda(\tau,s) = I_{b\lambda}(\tau,T), \tag{12}$$

where $I_\lambda(\tau, s)$ is the spectral radiative intensity in direction s at the optical thickness τ. $I_{b\lambda}(\tau, T)$ denotes the spectral radiative intensity of the blackbody. Integrating the RTE leads to

$$I_\lambda(x,\xi) = c\exp\left(\frac{\kappa_\lambda}{\cos\xi}x\right) - \frac{\kappa_\lambda}{\cos\xi}\exp\left(\frac{\kappa_\lambda}{\cos\xi}x\right) \times \int_{x_0}^{x} I_{b\lambda}(x, T)\exp\left(-\frac{\kappa_\lambda}{\cos\xi}x\right)\mathrm{d}x, \quad (13)$$

where ξ is the angle between the forward radiation and inward normal vector, c is the integration constant, and x_0 is an arbitrary constant value. With the following boundary conditions:

$$\begin{cases} I_\lambda(x,\xi) = 0, x = L, \\ I_\lambda(x,\eta) = 0, x = 0, \end{cases} \quad (14)$$

where η is the angle between the backward radiation and inward normal vector. Equation (13) can then be written as

$$I_\lambda(0,\xi) = \frac{\kappa_\lambda}{\cos\xi}\int_0^L I_{b\lambda}(x, T)\exp\left(-\frac{\kappa_\lambda}{\cos\xi}x\right)\mathrm{d}x, \quad (15)$$

$$I_\lambda(L,\eta) = \frac{\kappa_\lambda}{\cos\eta}\int_0^L I_{b\lambda}(x, T)\exp\left[-\frac{\kappa_\lambda}{\cos\eta}(L-x)\right]\mathrm{d}x. \quad (16)$$

Two surface types for interface 2 are considered: one is the opaque diffuse substrate surface, and the other is the semitransparent and specular-emerging surface.

(i) For an opaque diffuse substrate surface, a detailed derivation of the radiation in an arbitrary direction has been given in Ref. [30] and is not repeated here. The expression for the spectral radiative intensity in the direction of ϕ corresponding to β can be written as[30]

$$I_\lambda(\phi) = \left[I_\lambda(0,\beta) + \frac{I_\lambda}{1-K}\exp\left(-\frac{\kappa_\lambda L}{\cos\beta}\right)\right] \times \frac{[1-\rho_{s\lambda}(\beta, n_\lambda)]}{n_\lambda^2}, \quad (17)$$

where K is the rejection ratio, $\rho_{s\lambda}(\beta, n_\lambda)$ is the reflectivity of interface 1, β is the incident angle, and $\sin\phi/\sin\beta = n_\lambda$. I_λ is the first pseudo-source and its expression is

$$I_\lambda = \varepsilon_{L\lambda} I_{b\lambda}(L, T) + 2\rho_{L\lambda}\int_0^{\pi/2} I_\lambda(L,\eta)\sin\eta\cos\eta\,\mathrm{d}\eta + 2\int_0^{\theta_t} \rho_{L\lambda}\rho_{s\lambda}(\xi, n_\lambda) I_\lambda(0,\xi) \times \exp\left(-\frac{\kappa_\lambda L}{\cos\xi}\right)\sin\xi\cos\xi\,\mathrm{d}\xi + 2\int_{\theta_t}^{\pi/2} \rho_{L\lambda} I_\lambda(0,\xi)\exp\left(-\frac{\kappa_\lambda L}{\cos\xi}\right)\sin\xi\cos\xi\,\mathrm{d}\xi, \quad (18)$$

where $\rho_{L\lambda}$ and $\varepsilon_{L\lambda}$ are the reflectivity and emissivity of interface 2 and θ_t is the total reflection angle.

(ii) For a semitransparent and specular-emerging surface, the effective radiation of any point C on interface 2 ($x = L$) in the direction of CA (A is any point on the exit surface $x = 0$) can be divided into two parts:

a) the radiative intensity I_1 which is defined as the reflection radiative intensity of the forward radiation of the medium which goes along in the direction of CA, is expressed as

$$I_{1\lambda} = \rho_{s\lambda}(\eta, n_\lambda) I_\lambda(L,\eta); \quad (19)$$

b) the radiative intensity I_2 which is the reflection radiative intensity of the backward radiation of the medium through the semitransparent boundary after reaching point C and going along direction CA, is expressed as

$$I_{2\lambda} = \rho_{s\lambda}^2(\xi, n_\lambda) I_\lambda(0,\xi)\exp\left(-\frac{\kappa_\lambda L}{\cos\xi}\right). \quad (20)$$

Hence the expression for the first pseudo-source intensity of a semitransparent and specular-emerging surface can be written as

$$I_\lambda = I_{1\lambda} + I_{2\lambda}. \quad (21)$$

These two intensities correspond to the diffuse-light radiation, and therefore are called the first pseudo-source. The first pseudo source is transferred to the semitransparent surface after the attenuation of medium. A portion of this radiation passes to a basal surface after being reflected by a semitransparent surface, and then forms a second pseudo-source after being reflected again, and then forms a pseudo-source series. Therefore, the actual radiative intensity reaching point A along direction CA is

$$I_\lambda^+(0,\beta) = I_\lambda\left(0, \xi_{\xi=\beta}\right) + \frac{I_\lambda}{1-K}\exp\left(-\frac{\kappa_\lambda L}{\cos\beta}\right). \quad (22)$$

If interface 2 is an opaque diffuse substrate surface, the expression for K is

$$K = 2\rho_{L\lambda}\int_0^{\theta_t} \rho_{s\lambda}(\xi, n_\lambda)\exp\left(-\frac{2\kappa_\lambda L}{\cos\xi}\right)\sin\xi\cos\xi\,\mathrm{d}\xi + 2\rho_{L\lambda}\int_{\theta_t}^{\pi/2}\exp\left(-\frac{2\kappa_\lambda L}{\cos\xi}\right)\sin\xi\cos\xi\,\mathrm{d}\xi. \quad (23)$$

Whereas for a semitransparent and specular-emerging surface, the expression of K is written as

$$K = \rho_{s\lambda}^2(\xi, n_\lambda)\exp\left(-\frac{2\kappa_\lambda L}{\cos\xi}\right). \quad (24)$$

Then the spectral radiative intensity in direction ϕ corresponding to β can be written as

$$I_\lambda(\phi) = I_\lambda^+(0,\beta)\frac{[1-\rho_{s\lambda}(\beta, n_\lambda)]}{n_\lambda^2}. \quad (25)$$

Furthermore, the apparent spectral normal radiative intensity is

$$I_\lambda(0) = I_\lambda^+(0,0)\frac{[1-\rho_{s\lambda}(0, n_\lambda)]}{n_\lambda^2}. \quad (26)$$

Therefore, the expression of apparent spectral normal emissivity is

$$\varepsilon_{\perp}(\lambda, T) = \frac{I_{\lambda}(0)}{I_{\mathrm{b}\lambda}(T)}, \tag{27}$$

where I_{b} is the blackbody apparent spectral radiative intensity at temperature T and wavelength λ.

Moreover, if interface 2 is a semitransparent and specular-emerging surface, according to Beer's law, the expression for the spectral transmissivity can be written as

$$\tau(\lambda) = \frac{[1-\rho_{\mathrm{s}\lambda}(0,n_{\lambda})]^2 \exp(-\kappa_{\lambda} L)}{1-\rho_{\mathrm{s}\lambda}(0,n_{\lambda})^2 \exp(-2\kappa_{\lambda} L)}. \tag{28}$$

2.3.2. Inverse method

The optimization method associated with the inverse problem has been a topic of great interest. It has widely developed in the past decades, and its importance in applications derives partly from the advent of large computers and reliable numerical methods. Among these methods, the Particle Swarm Optimization (PSO) algorithm, which was first developed in 1995 by Eberhart and Kennedy,[31] receives a great deal of attention due to its superior computational stability, fast solution time, and efficiency in achieving a global minimum solution compared with the conventional gradient-based methods.[32–34] Our research group has exploited several PSO-based algorithms to determine the radiative properties, particle size distributions, and geometric conditions in various inverse radiation problems. The details of the PSO-based algorithms are available in Refs. [35]–[40] and are not repeated here.

The Stochastic Particle Swarm Optimization (SPSO) algorithm, which was first developed by Zeng and Cui,[41] is a PSO algorithm which ensures the convergence of the global optimum solution with a probability of one. This algorithm has been proved to be powerful in many optimal calculations, especially in parameter estimations.[35] In the present study, the SPSO is used to determine the spectral refractive index n_{λ} and absorption coefficient κ_{λ}. In the inverse problem, the apparent normal spectral emissivity $\varepsilon_{\perp}(\lambda)$ and transmissivity $\tau(\lambda)$ measured by the measurement system serve as the input for the inverse analysis to construct the objective function

$$F(n_{\lambda}, \kappa_{\lambda}) = \left[\frac{\varepsilon_{\perp}(\lambda) - \varepsilon'_{\perp}(\lambda)}{\varepsilon_{\perp}(\lambda)}\right]^2 + \left[\frac{\tau(\lambda) - \tau'(\lambda)}{\tau(\lambda)}\right]^2, \tag{29}$$

where the estimated apparent normal spectral emissivity $\varepsilon'_{\perp}(\lambda)$ and estimated transmissivity $\tau'(\lambda)$ are calculated by the PSAD method. The spectral refractive index n_{λ} and absorption coefficient κ_{λ} of the semitransparent material can be extracted by minimizing the above objective function through using the SPSO algorithm. A flowchart for this process is given in Fig. 3 and the specific inverse process is as follows(described briefly in the following):

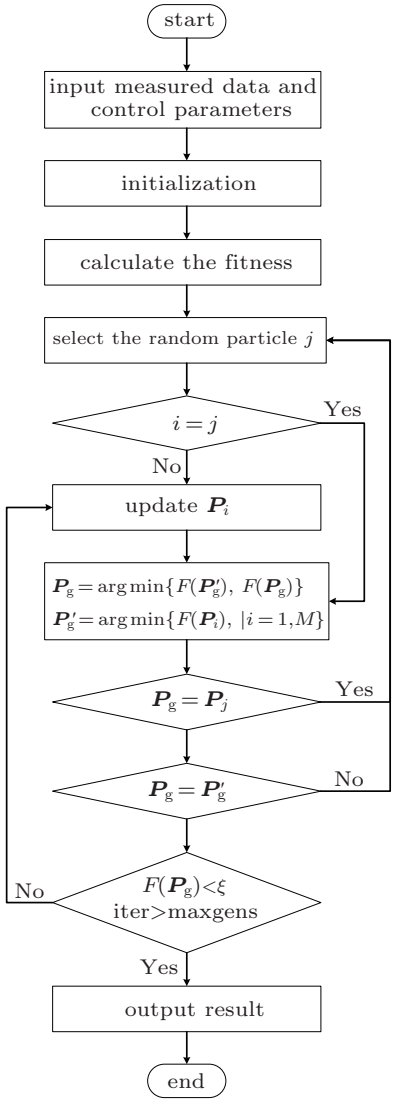


Fig. 3. Flowchart of retrieving the refractive index and absorption coefficient by SPSO.

Step 1 Input the apparent normal spectral emissivity $\varepsilon_{\perp}(\lambda)$ and transmissivity $\tau(\lambda)$ measured by the measurement system.

Step 2 Input the control parameters, and initialize a particle swarm where the position coordinate of each particle represents the spectral refractive index n_{λ} and absorption coefficient κ_{λ} of the medium.

Step 3 For each particle, calculate the estimated apparent normal spectral emissivity $\varepsilon'_{\perp}(\lambda)$ and estimated transmissivity $\tau'(\lambda)$ by the PSAD method, and then search the local best $\boldsymbol{P}_i$ and the global best $\boldsymbol{P}_{\mathrm{g}}$ by comparing its fitness value (i.e., the value of objective function).

Step 4 For each particle, update the particle position.

Step 5 Check the stop criterion. If the maximum number of generated sets is reached or the objective function value is less than the preset threshold, go to Step 6; otherwise, set the iteration index $t = t+1$, and loop to Step 3.

Step 6 Print out the optimal spectral refractive index and absorption coefficient.

2.3.3. Directional emissivity solving method

The spectral radiative intensity $I_\lambda(\theta)$ in direction θ can be calculated by Eq. (25) according to the retrieval spectral refractive index n_λ and absorption coefficient κ_λ of the semitransparent material in the above section. Then the apparent spectral directional emissivity of the semitransparent material in direction θ can be solved by using the PSAD method according to the following expression:

$$\varepsilon(\theta,\lambda,T)=\frac{I_\lambda(\theta)}{I_{b\lambda}(T)}, \tag{30}$$

where $I_{b\lambda}(T)$ is the blackbody spectral radiative intensity at temperature T and wavelength λ.

3. Verifications

3.1. Verification of the normal emissivity measurement system

To verify the reliability of the apparent normal spectral emissivity measurement device and measurement method based on the forward method, the apparent normal spectral emissivity of the infrared-grade sapphire is measured by using the measurement device and measurement method introduced in Section 2. The diameter and thickness of the sapphire sample are 15 mm and 1.0 mm, respectively, and the test temperature is 975 K. From Fig. 4, the present measurement result clearly shows good agreement with the result in Ref. [24], especially in a wavenumber range of 5 μm–10 μm. This proves that the apparent normal spectral emissivity measurement device and measurement method based on the direct method are reliable.

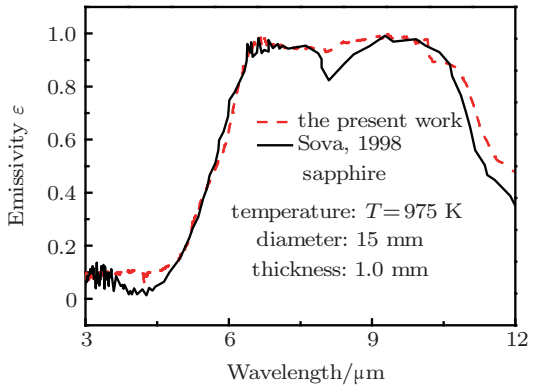


Fig. 4. (color online) Comparison of spectral emissivity of an infrared-grade sapphire sample at high temperature (T = 975 K) between the present work and Ref. [24].

3.2. Verification of the directional emissivity solving method

3.2.1. Verification of the forward problem solution of PSAD

To verify the reliability of the directional emissivity solving method, the direct problem model should be verified at first, with considering a semitransparent medium (see Fig. 2) and assuming interface 1 to be a semitransparent and specular-emerging surface and interface 2 to be an opaque diffuse substrate surface. The PSAD method is employed to determine the apparent spectral directional emissivity. The calculated results for two different cases are compared with results predicted by using the Vector Monte Carlo Method (VMCM) given in Ref. [42] (see Figs. 5 and 6). Clearly, the apparent spectral directional emissivity shows little variation over the viewing range of 0°–60°, whereas the emissivity sharply decreases as the angle exceeds 60°. Moreover, the results obtained using the PSAD method and VMCM agree well with each other, and hence demonstrate that calculating the apparent spectral directional emissivity using the PSAD method, given the refractive index and absorption coefficient of the medium, is reliable.

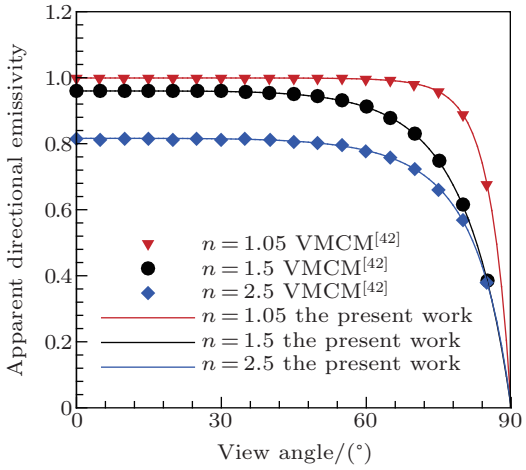


Fig. 5. (color online) Apparent directional emissivities under different refractive indices ($\varepsilon_{L\lambda}$=0.7, τ=3.0).

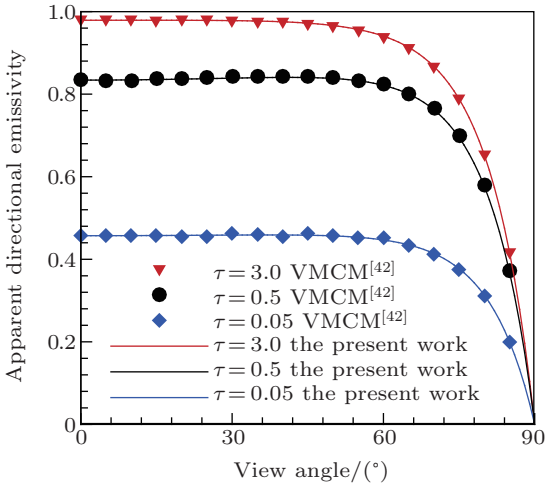


Fig. 6. (color online) Apparent directional emissivities under different optical thickness values ($\varepsilon_{L\lambda}$=0.2, n_λ=1.33).

3.2.2. Verification of the inverse method

The inverse problem model can be verified in a numerical simulated experiment based on the forward problem model. Assume that the refractive index and absorption coefficient of

the medium are known at first. Then the apparent normal emissivity and transmissivity can be predicted directly by using the PSAD method and serve as simulation experimental data for the inverse analysis. The refractive index and absorption coefficient of the medium can be retrieved by the SPSO algorithm to test the performance of the inverse method.

To demonstrate the effects of measurement errors on the retrieval results, the measured apparent normal emissivity and transmissivity with random errors are obtained by adding normal distribution errors to the exact apparent normal emissivity and transmissivity, that is,

$$S_{\mathrm{mea}} = S_{\mathrm{exact}} + \sigma\varsigma, \tag{31}$$

where S represents the apparent normal emissivity or transmissivity; ς is a normal distribution random variable with zero mean and standard unit deviation. The standard deviations of measured transmittance and reflectance σ for a $\gamma\%$ measured error at 99% confidence are determined from

$$\sigma = \frac{S_{\mathrm{exact}} \times \gamma\%}{2.576}. \tag{32}$$

For comparison, the relative error is defined as

$$\varepsilon_{\mathrm{rel}} = |P_{\mathrm{est}} - P_{\mathrm{exact}}|/P_{\mathrm{exact}}, \tag{33}$$

where P_{est} represents the retrieval refractive index or absorption coefficient, and P_{exact} denotes the exact refractive index or absorption coefficient.

As indicated in Fig. 2, assume that interfaces 1 and 2 are both semitransparent and specular-emerging surfaces, the thickness of the media is $L = 1$ m, the true values of the refractive index n_λ are 1.5, 2.5, and 3.5, and the true values of the absorption coefficient κ_λ are 0.5, 3.0, 7.0, and 10.0 m^{-1}. The refractive index and absorption coefficient are retrieved from the measured apparent normal emissivity and transmissivity by using the SPSO algorithm. The measurement errors are assumed to be 0%, 1%, and 3%, respectively. The retrieval results are listed in Table 2, where the system parameters of the SPSO algorithm are set to be as follows: the population size $M = 50$, the maximum iteration number $N_{\mathrm{t}} = 10000$, the tolerance of the objective function $\varepsilon_0 = 10^{-8}$, the search range for the absorption coefficient $\kappa_\lambda \in [0.0, 15]$ m^{-1}, and the search range for the refractive index $n_\lambda \in [1.0, 5.0]$.

Table 2. Retrieval results of absorption coefficient and refractive index.

Inverse parameter	True value	$\gamma = 0$		$\gamma = 1\%$		$\gamma = 3\%$	
		Retrieval value	$\varepsilon_{\mathrm{rel}}\%$	Retrieval value	$\varepsilon_{\mathrm{rel}}\%$	Retrieval value	$\varepsilon_{\mathrm{rel}}\%$
n	1.5	1.5001	0.0067	1.5329	2.1933	1.6198	7.9867
κ/m^{-1}	0.5	0.5000	0.0000	0.5007	0.1400	0.4960	0.8000
n	1.5	1.5000	0.0000	1.5329	2.1933	1.5967	6.4467
κ/m^{-1}	3.0	3.0002	0.0067	2.9998	0.0067	2.9995	0.0167
n	1.5	1.5000	0.0000	1.5315	2.1000	1.5924	6.1600
κ/m^{-1}	7.0	6.9973	0.0386	6.9995	0.0071	6.9967	0.0471
n	1.5	1.5000	0.0000	1.5314	2.0933	1.5924	6.1600
κ/m^{-1}	10.0	10.014	0.1400	9.9696	0.3040	9.9270	0.7300
n	2.5	2.4999	0.0040	2.5301	1.2040	2.5868	3.4720
κ/m^{-1}	0.5	0.5000	0.0000	0.5001	0.0200	0.4978	0.4400
n	2.5	2.5000	0.0000	2.5258	1.0320	2.5778	3.1120
κ/m^{-1}	3.0	3.0000	0.0000	2.9998	0.0067	2.9995	0.0167
n	2.5	2.5000	0.0000	2.5248	0.9920	2.5747	2.9880
κ/m^{-1}	7.0	7.0040	0.0571	7.0081	0.1157	7.0085	0.1214
n	2.5	2.5000	0.0000	2.5248	0.9920	2.5748	2.9920
κ/m^{-1}	10.0	9.9776	0.2240	10.048	0.4800	9.8698	1.3020
n	3.5	3.4999	0.0029	3.5280	0.8000	3.6044	2.9829
κ/m^{-1}	0.5	0.5000	0.0000	0.5007	0.1400	0.4963	0.7400
n	3.5	3.5000	0.0000	3.5277	0.7914	3.5838	2.3943
κ/m^{-1}	3.0	2.9998	0.0067	2.9998	0.0067	2.9995	0.0167
n	3.5	3.5000	0.0000	3.5268	0.7657	3.5791	2.2600
κ/m^{-1}	7.0	6.9915	0.1214	7.0097	0.1386	7.1364	1.9486
n	3.5	3.5000	0.0000	3.5268	0.7657	3.5810	2.3143
κ/m^{-1}	10.0	9.9946	0.0540	9.9729	0.2710	9.9728	0.2720

Clearly from Table 2, the absorption coefficient and refractive index can be retrieved accurately without measurement error, given that a maximum relative retrieval error is only 0.224%. The relative retrieval errors increase with increasing measurement error, but they are all within a reasonable range, and even with 3% measurement error, the maximum relative retrieval error of the refractive index is less than 8% and the relative retrieval error of the absorption coefficient is only 1.95%. Therefore, the reasonable retrieval results for the absorption coefficient and refractive index can be obtained

by this method even with measurement errors, which demonstrates that the inverse problem model is effective and reliable.

Moreover, from Table 2, compared with the refractive index, the absorption coefficient has high accuracy. This is primarily attributed to the fact that the sensitivities of the normal emissivity and transmissivity to the refractive index are both relatively small. In the present research, the sensitivity coefficient of the normal emissivity or transmissivity with respect to a_k is estimated from the finite difference approximation:[43]

$$\chi_{a_k}(S) = \left.\frac{\partial S}{\partial a_k}\right|_{a_k=a_0} = \frac{S(a_0 + a_0\Delta) - S(a_0)}{a_0\Delta}, \qquad (34)$$

where a_k represents either the absorption coefficient κ or the refractive index; Δ denotes the percentage of small change in parameter a_k, which is taken as $\Delta = 0.5\%$, and S is the normal emissivity or transmissivity. The sensitivity coefficients of the normal emissivity $\chi_\kappa(\varepsilon)$ and transmissivity $\chi_\kappa(\tau)$ with respect to the absorption coefficient κ are plotted in Fig. 7. The sensitivity coefficients of the normal emissivity $\chi_\kappa(\varepsilon)$ and transmissivity $\chi_n(\tau)$ with respect to refractive index n are presented in Fig. 8.

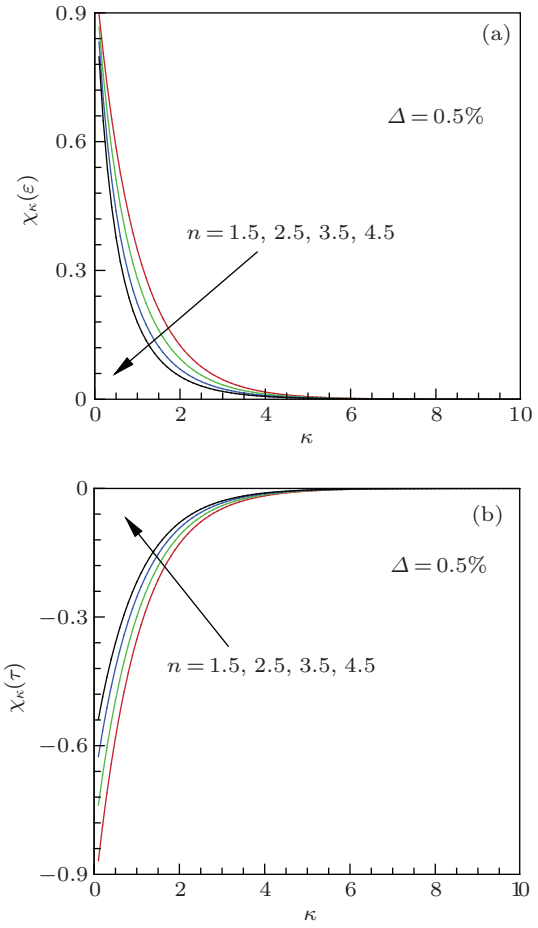


Fig. 7. (color online) Variations of sensitivity coefficients of (a) the normal emissivity $\chi_\kappa(\varepsilon)$ and (b) transmissivity $\chi_\kappa(\tau)$ with absorption coefficient κ.

As shown in Fig. 7, the absolute values of the sensitivity coefficients of the normal emissivity and transmissivity with respect to absorption coefficient sharply decrease with increasing absorption coefficient. Hence the relative retrieval error of the absorption coefficient increases with increasing absorption coefficient. Figure 8 shows that the absolute values of the sensitivity coefficients of the normal emissivity and transmissivity with respect to the refractive index increase with increasing refractive index when the absorption coefficient is small, which causes the relative retrieval error of the refractive index to decrease with increasing refractive index. However, the sensitivity coefficients of the normal emissivity and transmissivity with respect to refractive index are very small and vary little with the refractive index when the absorption coefficient is large, especially for the sensitivity coefficients of the transmissivity with respect to refractive index, which leads to the relative retrieval error of the refractive index varying little with the refractive index in this case.

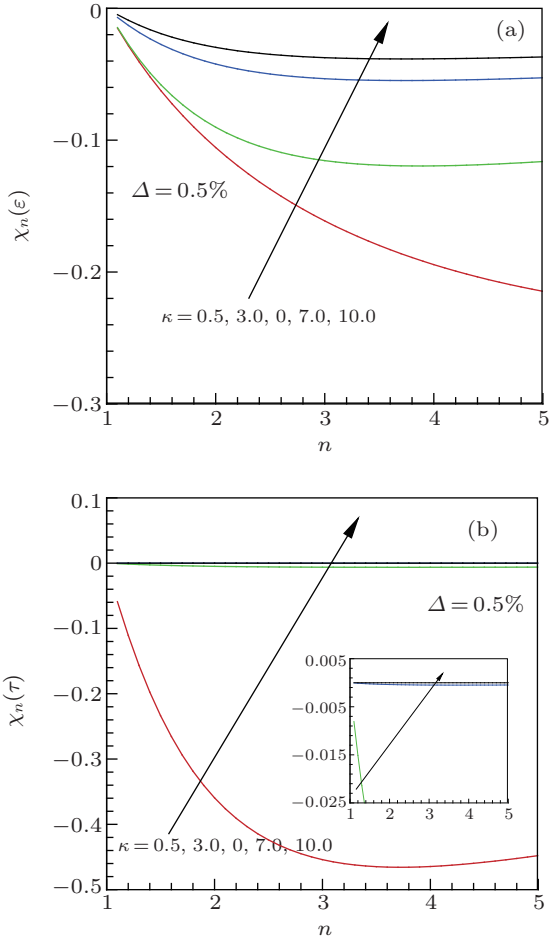


Fig. 8. (color online) Variations of sensitivity coefficients of (a) the normal emissivity $\chi_n(\varepsilon)$ and (b) transmissivity $\chi_n(\tau)$ with refractive index n.

4. Measurement results

Based on the above verification, the apparent spectral directional emissivity of a sapphire sample is measured using this measurement system. The sapphire sample used in the experiment is a wafer sample, and the diameter is 50 mm, the thickness is 0.4 mm, the test temperature is 773 K, and the

range of measurable wavelength is 3 μm–12 μm. The apparent normal spectral emissivity and transmissivity of this sample are measured first (see Fig. 9). From the plots, we find that the apparent normal spectral emissivity and transmissivity of this sapphire sample vary little with wavelengths in a range of 3 μm–4 μm, emissivity is around 0.2, and transmissivity is around 0.7. If the wavelength is in a range of 4 μm–7.5 μm, the normal emissivity sharply increases with increasing wavelength, whereas the transmissivity sharply decreases with increasing wavelength. The transmissivity is very small and remains at 0.03 for wavelengths larger than 7.5 μm. However, the normal emissivity is around 0.9 for wavelengths in a range of 7.5 μm–10.5 μm, and the normal emissivity sharply decreases with increasing wavelength for wavelengths larger than 7.5 μm. The trends of the apparent normal spectral emissivity and transmissivity with wavelength are consistent with the measurement data in Ref. [44].

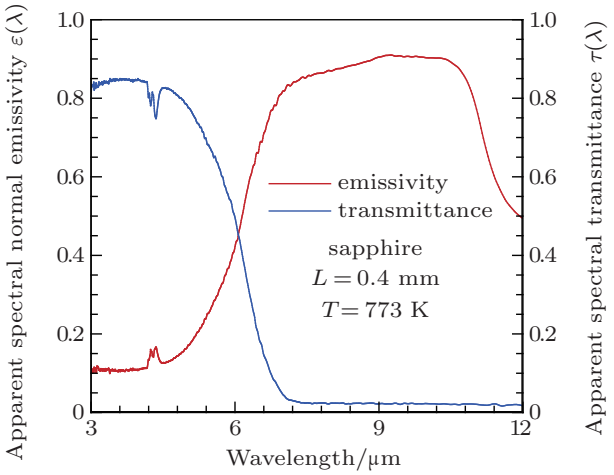


Fig. 9. (color online) Plots of apparent normal spectral emissivity and transmissivity versus wavelength of the sapphire sample.

According to the apparent normal spectral emissivity and transmissivity of the sample (Fig. 9), the apparent spectral directional emissivity of the sapphire sample can be obtained using the inverse method developed in this study. Initially, the spectral refractive index n_λ and absorption coefficient κ_λ are retrieved from the measured apparent normal emissivity and transmissivity by using the SPSO algorithm, and the parameter settings of the SPSO algorithm are as follows: population size M=50; maximum iteration number $N_t = 10^4$; tolerance of the objective function $\varepsilon_0 = 10^{-8}$; searching range for the absorption coefficient $\kappa_\lambda \in [0.0, 4000]$ m^{-1}; and searching range for the refractive index $n_\lambda \in [1.0, 5.0]$. The apparent spectral directional emissivities of sapphire at different viewing angles can be calculated using the PSAD method according to the refractive index and absorption coefficient, and the results are shown in Fig. 10.

As shown in Fig. 10, it can be seen that the variation tendencies of the apparent spectral directional emissivity at different viewing angles with the wavelength are consistent with each other. Moreover, the apparent spectral directional emissivity for the sample changes little for a viewing angle of less than 60°, but sharply decreases with increasing viewing angle if the viewing angle is larger than 60°. This trend agrees with those given in Figs. 5 and 6. Furthermore, for a range of 3 μm–12 μm, the apparent spectral hemisphere emissivity of the sample and the apparent band directional emissivity have also been calculated, and the results are shown in Figs. 11 and 12 respectively. From Fig. 11 it can be seen that the variation of the apparent spectral hemisphere emissivity with wavelength is quite similar to that of the apparent spectral directional emissivity of the sample. Figure 12 shows that the apparent spectral band directional emissivity of the sample is around 0.4 and changes little for a viewing angle of less than 60°, but sharply decreases with increasing viewing angle if the viewing angle is larger than 60°, which agrees with those trends in Fig. 10.

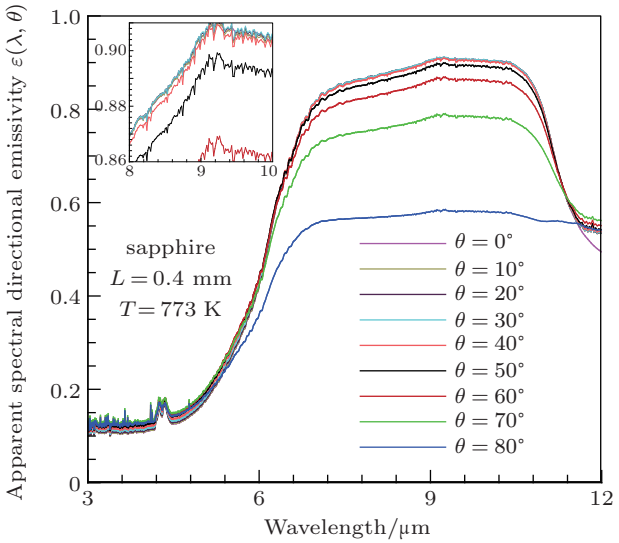


Fig. 10. (color online) Plots of apparent spectral directional emissivity versus wavelength for different θ values of the sapphire sample.

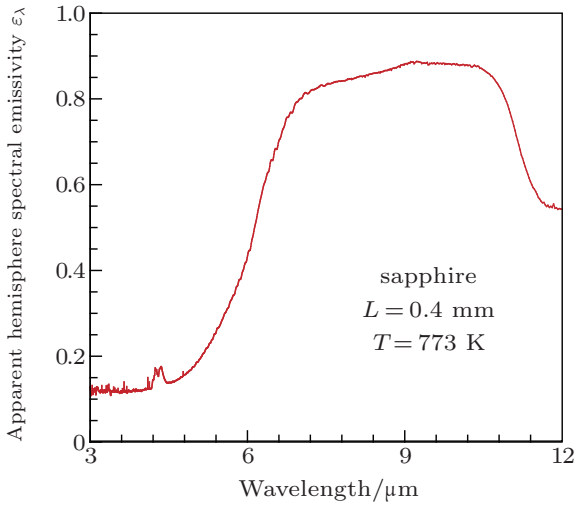


Fig. 11. (color online) Variation of apparent spectral hemisphere emissivity with wavelength of the sapphire sample.

In order to further verify the present inverse method, the direct measurement method is used to measure the apparent spectral directional emissivities of the same sapphire sample at the same test temperature for viewing angles 30° and 60°. A comparison between the emissivity results obtained by the proposed inverse method and the measurements is shown in Fig. 13. Good agreement is obtained between the apparent spectral directional emissivity obtained by the proposed inverse method and the experimental one, which proves that the apparent spectral directional emissivity measurement technology based on the inverse method is reliable.

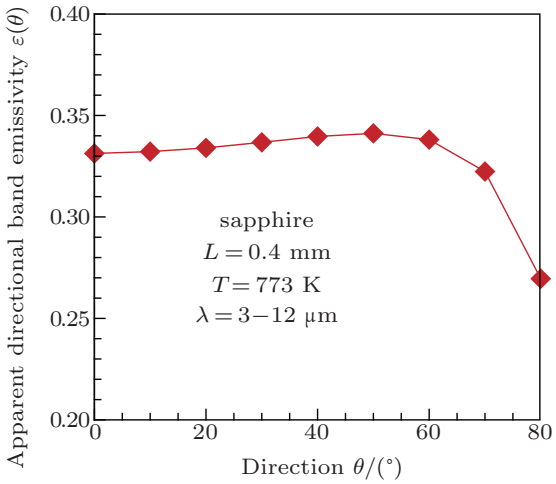


Fig. 12. (color online) Variation of apparent band directional emissivity with direction of the sapphire sample.

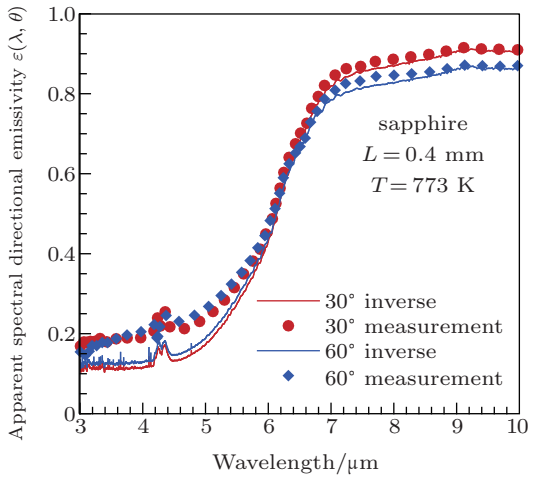


Fig. 13. (color online) Comparison between the apparent spectral directional emissivity obtained by the proposed inverse method and that by the direct measurement method.

5. Conclusions

An inverse estimation method and corresponding measurement system are developed to measure the apparent spectral directional emissivities of semitransparent materials based on the direct measurement method. The apparent normal spectral emissivity and transmissivity are initially measured using the measurement system, which serves as input for the inverse analysis. The refractive index and absorption coefficient of the semitransparent material are retrieved using the PSAD method as the forward method and using the SPSO algorithm as the inverse method. Finally, the apparent spectral directional emissivities of semitransparent materials can be calculated by the PSAD method according to the retrieval refractive index and absorption coefficient. The innovation of this study is that the measurement system combined with the inverse calculation, reduces the complexity and expands the scope of the measurement system, and allows the measurements of the emissivity for arbitrary direction without blind spots in the viewing range. The main technical indicators of the measurement system include a heating temperature range for the sample of 300 K–1773 K, a spectral range of 2.5 μm–25 μm, and a viewing range of 0°–90°. The reliabilities of the apparent normal spectral emissivity and transmissivity measurement data are verified by comparing the experimental results with those in other references. The feasibility of calculating apparent spectral directional emissivity using the PSAD method is verified by comparing the calculation with the vector Monte Carlo method. By numerically simulated experiments, the apparent normal emissivity and transmissivity can be simulated directly using the PSAD method and serve as simulation experiment data for the inverse analysis. The refractive index and absorption coefficient of the medium can be retrieved by the SPSO algorithm according to the simulated experimental data. The results show that the reasonable retrieval results for the absorption coefficient and refractive index can be obtained by this method even with measurement errors, and demonstrate that the inverse model is reasonable and reliable. After completing the verification of the apparent spectral directional emissivity measurement system, the apparent spectral directional emissivity of sapphire at 773 K is measured by this measurement system, the spectral range being 3 μm–12 μm and the viewing range being 0°–90°. The results obtained show that the proposed method has promise in measuring the directional spectral emissivities of semitransparent materials, which paves the way for a new directional spectral emissivity measurement strategy.

References

[1] Campo L del, Pérez-Sáez R B, Esquisabel X, Fernández I and Tello M J 2006 *Rev. Sci. Instrum.* **77** 113111
[2] Shi D H, Liu Y F, Sun J F, Zhu Z L and Liu H 2012 *Int. J. Heat Mass Transfer* **55** 3344
[3] Ishii J and Ono A 2000 *SPIE* **4103** 126
[4] Dai J M and Wang X B 2007 *Acta Metrologica Sinica* **28** 232
[5] Zhang Y F, Dai J M, Zhang L and Pan W D 2012 *Opt. Eng.* **52** 087107
[6] Wang F Q, Shuai Y, Yuan Y and Liu B 2012 *Materials and Design* **33** 284
[7] Wang F Q, Tan J Y and Wang Z Q 2014 *Energy Conversion and Management* **83** 159
[8] Wang F Q, Tan J Y, Shuai Y, Tan H P and Leng Y 2014 *Solar Energy* **108** 348

[9] Zhang S D, Xia X L, Dai G L, Yu M X and Yan W X 2012 *J. Eng. Thermophys.* **33** 1032

[10] Cezairliyan A and Laylor J 1997 *Journal of Research of the National Bureau of Standards, Section A, Physics and Chemistry* **81** 251

[11] Fu T R, Liu J F, Tang J Q, Duan M H, Zhao H and Shi C L 2014 *Infr. Phys. Technol.* **66** 49

[12] Thevenet J, Siroux M and Desmet B 2010 *Appl. Therm. Eng.* **30** 753

[13] Wen C D and Chai T Y 2011 *Appl. Therm. Eng.* **31** 2414

[14] Yang W, Fan A W, Wan J L and Liu W 2015 *Appl. Therm. Eng.* **3** 8

[15] Wang H, Chen D J, Wang G L, Long Y S, Luo J, Liu L P and Yang Q T 2013 *Measurement* **46** 4023

[16] Modest M F 2003 *Radiative heat transfer* (New York: McGraw-Hill)

[17] Fu T R, Tan P and Pang C H 2012 *Measurement Science and Technology* **23** 025006

[18] Fu T R and Tan P 2012 *ASME J. Heat Transfer* **134** 111601

[19] Fu T R, Tan P and Zhong M H 2012 *Experimental Thermal and Fluid Science* **40** 159

[20] Fu T R, Tan P and Duan M H 2015 *Measurement Science and Technology* **26** 015003

[21] Lindermeir E, Tank V and Haschberger P 1992 *Proc. SPIE* **1682** 354

[22] Tank V 1999 *Journal of Molecular Structure* **482** 545

[23] Dai J M, Wang X B and Yuan J B 2005 *J. Phys.* **13** 63

[24] Sova R M, Linevsky M J, Thomas M E and Mark F F 1998 *Infr. Phys. Technol.* **39** 251

[25] González-Fernández L, Campo L del, Pérez-Sáez R B and Tello M J 2012 *J. Alloys Compd.* **513** 101

[26] Rozenbaum O, Meneses D, Auger Y, Chermanne S and Echegut P 1999 *Rev. Sci. Instrum.* **70** 4020

[27] Lee G W, Jeon S, Yoo N J, Park C W, Park S N, Kwon S Y and Lee S H 2011 *Int. J. Thermophys.* **32** 1234

[28] Ishii J and Ono A 2001 *Measurement Science and Technology* **12** 2103

[29] Huang Y, Xia X L, Tan H P and Yu Q Z 1999 *J. Infr. Millim. Waves* **18** 276

[30] Huang Y, Xia X L, Tan H P and Yu Q Z 1999 *Chin. J. Comput. Phys.* **16** 505

[31] Kennedy J and Eberhart R C 1995 *Particle swarm optimization* (New York: IEEE)

[32] Kraszewski M, Strakowski M, Plucinski J and Kosmowski B B 2015 *Appl. Opt.* **54** 76

[33] Yuan Y, Yi H L, Shuai Y, Liu B and Tan H P 2011 *Atmospheric Environment* **45** 4892

[34] Yoon K B, Park S J and Kim T K 2013 *Appl. Opt.* **52** 5533

[35] Qi H, Ruan L M, Zhang H C, Wang Y M and Tan H P 2007 *Int. J. Therm. Sci.* **46** 649

[36] Qi H, Ruan L M, Wang S G, Shi M and Zhao H 2008 *Chin. Opt. Lett.* **6** 346

[37] Qi H, Ruan L M, Shi M, An W and Tan H P 2008 *J. Quantum Spectrosc. Radiat. Transfer* **109** 476

[38] Zhang B, Qi H, Ren Y T, Sun S C and Ruan L M 2013 *Int. J. Heat Mass Transfer* **66** 507

[39] Zhang B, Qi H, Ren Y T, Sun S C and Ruan L M 2014 *Journal of Quantitative Spectroscopy & Radiative Transfer* **133** 351

[40] Qi H, Ren Y T, Lew Z Y and Ruan L M 2015 *Appl. Opt.* **54** 5234

[41] Zeng J C and Cui Z H 2004 *J. Comput. Res. Develop.* **41** 1333

[42] Wang C H 2013 *Temperature measurement using multispectral radiation thermometry and the apparent radiation characteristics for semi-transparent medium* (Harbin: Harbin Institute of Technology)

[43] Kurpisz K and Nowak A J 1995 *Inverse thermal problems* (Computational Mechanics Publication)

[44] Moriaki W, Keie K and Takehisa S 2007 *Physical properties and data of optical materials* (Florida: CRC Pr I Llc)